ACS Catalysis

Research Article

pubs.acs.org/acscatalysis

PdAg Alloy Nanowires: Facile One-Step Synthesis and High Electrocatalytic Activity for Formic Acid Oxidation

Yizhong Lu[†,‡] and Wei Chen*[,†]

[†]State Key Laboratory of Electroanalytical Chemistry, Changchun Institute of Applied Chemistry, Chinese Academy of Sciences, Changchun 130022, Jilin, China

[‡]Graduate School of the Chinese Academy of Sciences, Beijing 100039, China

ABSTRACT: Bimetallic alloy PdAg nanowires were synthesized by a facile one-step wet chemical strategy. The unique nanostructure with large surface area and active surface (111) planes make them promising electrocatalysts for direct-liquid fuel cells. The electrochemical studies indicated that the PdAg alloy nanowires exhibit enhanced electrocatalytic activity toward formic acid oxidation with larger oxidation current density, higher tolerance to CO poisoning, and more negative onset potential in comparison with the commercial Pd/C catalysts. At the same potentials, the as-synthesized PdAg nanowires show higher long-term stability than Pd/C catalysts in the chronoamperometric analyses. The electron transfer kinetics of HCOOH oxidation on the PdAg nanowires was studied with electrochemical impedance spectroscopy (EIS). It was found that the charge transfer resistance (R_{CT}) of formic acid oxidation on PdAg nanowires is much smaller than that obtained from a Pd/C catalyst, which suggests that the electron-transfer kinetics for formic acid oxidation at the synthesized PdAg nanowires is highly facilitated. The present work highlights the facile synthesis of the homogeneous PdAg alloy nanowires and their potential application as anode electrocatalyst of fuel cells.

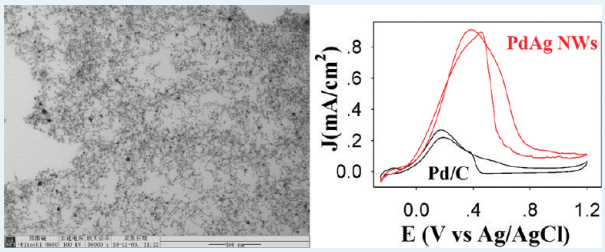

KEYWORDS: *PdAg nanowire, electrocatalysis, fuel cell, formic acid oxidation, electrochemical impedance spectroscopy*

1. INTRODUCTION

Direct liquid fuel cells, including direct methanol fuel cells (DMFCs) and direct formic acid fuel cells (DFAFCs), are considered to be one of the promising clean energy sources with high energy conversion efficiency and low environmental pollution.[1−4] For fuel cells, platinum has been widely used as electrocatalyst because it has the highest catalytic activity among the anode metal catalysts for electro-oxidation of small organic fuels and the cathode catalysts for oxygen reduction.[5−9] However, with platinum as an anode catalyst, the surface is usually heavily poisoned by the strong adsorption of CO intermediates produced during the oxidation of organic fuels, resulting in the lowering of catalytic performance. Compared to the pure platinum electrocatalyst, Pt-based alloys with other transition metals, especially the nanostructured materials, exhibit higher performance because of the so-called bifunctional mechanism.[10,11] However, because of the high cost and the limited world supply of platinum, recent extensive research efforts have been devoted to the development of nonplatinum electrocatalysts with comparable catalytic properties. Among the metal-based catalysts studied to date, palladium has been considered to be a promising alternative because of its similar properties to platinum but much lower cost than platinum.[12] More importantly, in situ spectroelectrochemical studies showed that only little or no CO is formed for formic acid and other organic small molecule oxidation on the surfaces of Pd single crystals and other Pd-based catalysts.[13−17] That is, different from the so-called dual pathway mechanism on Pt-based electrocatalysts, the mechanism of a direct oxidation pathway to CO_2 through an active intermediate was proposed for formic acid oxidation at Pd surfaces with no or very low CO poisoning. Recent studies also revealed that Pd at the nanometer-sized scale can catalyze the formic acid oxidation at the anode of polymer electrolyte membrane fuel cells (PEMFCs) with greater resistance to CO poisoning than Pt catalysts.[18] In addition to much work concentrated on Pd single crystals,[19] Pd films[20] and Pd or Pd-based nanoparticles, various Pd nanostructured materials, such as Pd nanowires,[21] Pd nanoflowers,[22] Pd nanotrees,[23] Pd nanoplate arrays,[23] and porous Pd nanorods,[24] have also been synthesized and studied as anode electrocatalysts for methanol and other organic molecule oxidation.

For the nanostructured electrocatalysts, it is well-known that the catalytic performance is largely dependent on their surface structures, such as the surface facets, particle size, particle shape, and so forth. Recently, Xia and co-workers[25] synthesized Pd−Pt bimetallic nanodendrites which exhibit enhanced catalytic activity for oxygen electro-reduction. Extensive studies have showed that one-dimensional bimetallic nanowires or nanotubes exhibit enhanced electrocatalytic activity for fuels anodic

Received: October 17, 2011
Revised: November 24, 2011
Published: November 29, 2011

 © 2011 American Chemical Society dx.doi.org/10.1021/cs200538g | ACS Catal. 2012, 2, 84−90

oxidation and oxygen cathodic reduction because of the large specific interface areas. However, in the previous studies, the most used method to prepare bimetallic nanowires is the metal seed-based epitaxial synthetic route, in which metal seeds are first synthesized and nanowires grow subsequently onto the metal core nanoparticles.[26−30] For instance, Yuan et al. synthesized Pt−Rh[26] and Pd−Pt[27] heterostructured ultrathin nanowires by using Pd and Rh nanocubes as seeds, respectively. Because of the lower standard reduction potential of Ag^+/Ag (+ 0.7991 V versus NHE) than that of Pd^{2+}/Pd (+ 0.915 V), galvanic displacement reaction is often adopted to synthesize heterostructured PdAg bimetallic one-dimensional nanomaterials by using Ag nanotubes or nanowires as templates.[31−34] The heterostructured bimetallic nanowires/nanotubes synthesized with these methods have two obvious disadvantages. (1) From the point of materials synthesis, two steps were needed to obtain the final materials, including seeds preparation and the following deposition of the second metal to synthesize bimetallic nanowires/nanotubes; (2) From the viewpoint of catalytic activity of anode Pt-based electrocatalysts, heterostructures are not ideally favorable for CO-tolerance during organic small molecule oxidation. Given these considerations, synthesis of a homogeneous alloy instead of heterostructured bimetallic nanowires with a facile method is promising for designing novel nanostructured fuel cell electrocatalysts.[35−37]

To this end, we report here a facile one-pot solution-phase synthesis of PdAg alloy nanowires. The unique nanowires were produced by the coreduction of Pd and Ag precursors in the presence of PVP. Among the various bimetallic nanoparticles fabricated to date, PdAg materials are very fascinating because of their excellent catalytic activities for a variety of chemical reactions. The as-prepared PdAg nanowires exhibited excellent electrocatalytic activity toward formic acid oxidation. Importantly, the PdAg nanowires were found to be of alloy structure and were synthesized by a one-step based method. The structures of the PdAg nanowires were characterized in detail with transmission electron microscopy (TEM), high- resolution transmission electron microscopy (HRTEM), X-ray diffraction (XRD), and energy-dispersive X-ray analysis. The electrocatalytic activity of the PdAg Nanowires toward formic acid was examined with electrochemical voltammetry and impedance measurements; the results showed that the synthesized PdAg nanowires exhibit excellent catalytic activity with high current density and high tolerance to CO poisoning. The catalytic performance of alloy PdAg nanowires were also compared with commercial Pd/C catalysts.

2. EXPERIMENTAL SECTION

2.1. Chemicals and Materials. Silver nitrate ($AgNO_3$, ≥99.8% Beijing Chemical Reagent), poly (vinyl pyrrolidone (PVP, M_w ≈55,000, Aldrich), ethylene glycol (EG, A. R. grade, Beijing Chemical Reagent), Palladium(II) nitrate dihydrate ($Pd(NO_3)_2{\cdot}2H_2O$, CP. Sinopharm Chemical Reagent Co. Ltd.), perchloric acid ($HClO_4$, A.R. grade, Tianjin Chemical Reagent), and formic acid (HCOOH, A.R. grade, Beijing Chemical Reagent) were used as received. 5% Pd/C was purchased from Alfa Aesar, and water was supplied by a Water Purifier Nanopure water system (18.3 MΩ cm).

2.2. Synthesis of PdAg Nanowires. In a typical synthesis, a EG solution of poly(vinyl pyrrolidone) (0.6 mmol, 5 mL, MW = 55,000, Aldrich) was placed in a three-neck flask (equipped with a reflux condenser and a Teflon-coated magnetic stirring bar) and heated with an oil bath at 170 °C for 1 h. Meanwhile, silver nitrate (0.05 mmol, 8.5 mg) and Pd $(NO_3)_2{\cdot}2H_2O$ (0.05 mmol, 13.32 mg) were codissolved in 2 mL of nanopure water at room temperature, and the solution was then added to the EG solution rapidly using a syringe. Heating and stirring continued for an additional 1 h. After the solution was cooled to room temperature, 30 mL of acetone was added to precipitate the products, and then centrifuged at a rate of 8000 rpm for 10 min. The synthesized materials were washed at least three times with acetone. The final black precipitation was redispersed into water for further use.

2.3. Electrochemistry. Before each experiment, the glassy carbon (GC) electrode (3.0 mm in diameter) was first polished with alumina slurries (Al_2O_3, 0.3 μm) powder on a polishing cloth to obtain a mirror finish, followed by sonication in 0.1 M HNO_3, 0.1 M H_2SO_4, and pure water for 10 min, successively. To prepare a catalyst-coated GC electrode, 10 μL of the 1 mg/mL suspension of the PdAg nanowires or commercial Pd/C catalyst in pure water and 5 μL of 5 wt % Nafion solution were drop-coated on a polished GC electrode. The nanowires-coated GC electrode was dried in vacuum at room temperature and then subjected to Ar plasma (200 W, 0.3 Torr) cleaning for 10 min to remove the organic residues. The electrodes prepared from PdAg nanowires and Pd/C catalysts were denoted as PdAg-NW/GC and Pd/GC, respectively.

Voltammetric measurements were carried out with a CHI 750D electrochemical workstation. The PdAg-NW/GC or Pd/GC electrode prepared above was used as the working electrode. An Ag/AgCl (in 3 M NaCl, aq.) and a Pt coil were used as the reference and counter electrodes, respectively. All electrode potentials in the present study were referred to this Ag/AgCl reference. The solutions were deaerated by bubbling ultrahigh-purity N_2 for 20 min and protected with a nitrogen atmosphere during the entire experimental procedure. All electrochemical experiments were carried out at room temperature.

2.4. Material Characterization. Powder XRD was performed on a D/Max 2500 V/PC powder diffractometer using Cu−Kα radiation with a Ni filter (λ = 0.154059 nm at 30 kV and 15 mA). The morphology and the crystal structure of the PdAg nanowires were analyzed with a HITACHI H-600 Analytical Transmission Electron Microscope with an accelerating voltage of 100 KV. UV−vis spectra were recorded on a VARIAN CARY 50 UV−vis spectrophotometer. High-resolution TEM (HRTEM) images, high-angle annular dark-field scanning transmission electron microscopy (HAADF-STEM) images, and element analysis mapping were carried out on a JEM-2010(HR) microscope operated at 200 kV.

3. RESULTS AND DISCUSSION

3.1. Characterization of PdAg Nanowires. The morphologies of the as-synthesized materials are characterized with transmission electron microscopy (TEM) measurements. Figure 1A−B shows the TEM images of final products at different magnifications. It can be seen that, with the present one-pot preparation method, uniform nanowires in high yield were obtained. The length of such nanowires can be up to 200 nm with average diameters of 5−8 nm. The morphology of such ultrathin nanowires is very similar to that of other two-step synthesized bimetallic nanowires with seed-mediated epitaxial growth methods.[26,27] So the present report provides a facile route for preparing metal nanowires. From the energy-dispersive X-ray analysis shown in Figure 1C, both Pd and Ag are present in the nanowire materials in addition to the Cu

dx.doi.org/10.1021/cs200538g | ACS Catal. 2012, 2, 84−90

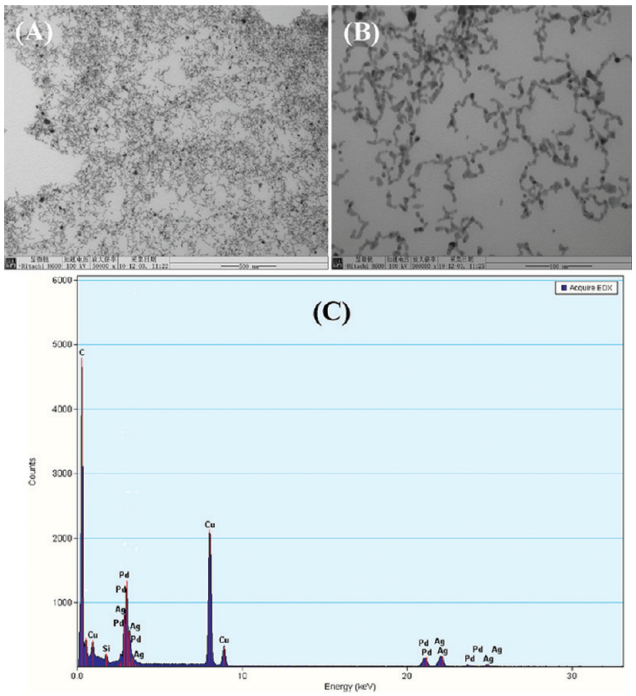

Figure 1. (A-B) TEM micrographs of PdAg nanowires at different magnifications. The scale bars are (A) 500 nm and (B) 100 nm. (C) Energy-dispersive X-ray analysis (EDX) of the PdAg nanowires.

substrate. The average ratio of Pd to Ag is determined to be 45:55 based on the EDX measurement. The PdAg nanowires exhibits a typical Mie exponential decay absorption profile in UV−vis measurements (not shown here).

It should be noted that heterostructures were usually obtained in the previous synthesis of bimetallic nanowires with seed-mediated epitaxial growth methods. To investigate the crystal structures and the element distribution of the synthesized PdAg nanowires, high-resolution TEM (HRTEM) analyses were also performed. Figure 2A−B depict the HRTEM images at different magnifications, in which worm-like nanowires were uniformly dispersed. In Figure 2B, well-resolved lattice fringes can be seen clearly. By careful measurements, it was found that there is mainly one type of lattice fringes with interplanar spacing of 2.34 Å, which is ascribed to the (111) planes. The distribution of Pd and Ag in the whole nanowires was studied with element analysis mapping. Figure 2C−F shows the HAADF-STEM image and selected-area element analysis maps of Pd, Ag and the overlay. The element maps reveal that the elements of Pd and Ag are homogeneously dispersed in the PdAg nanowires, indicating the formation of alloy structure. Interestingly, like the bimetallic nanowires synthesized with nanoparticle seed-mediated method, it can be seen from Figure 2A−B that the present as-synthesized PdAg nanowires are composed with multiple crystalline domains. However, different from the monometallic domains dispersed in the heterostructured nanowires, alloy domains were formed with the present synthesis method. The HRTEM and elements analysis strongly suggest that in the forming process of

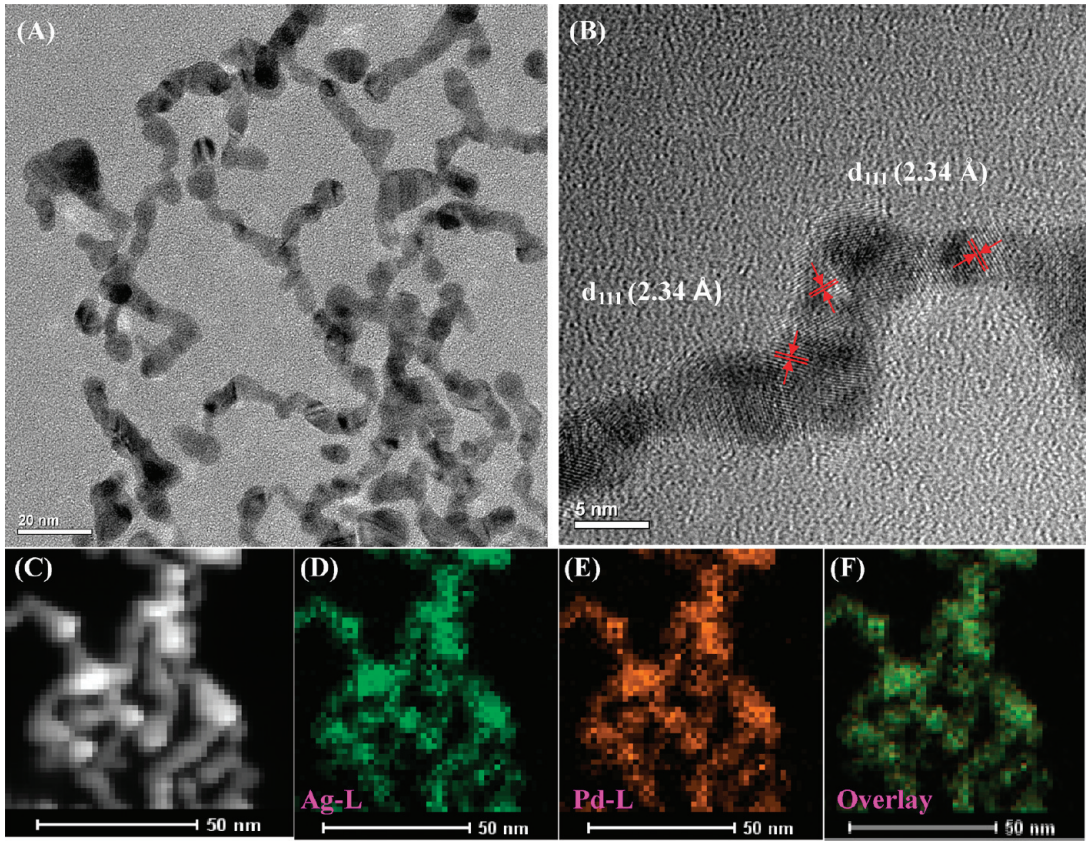

Figure 2. (A-B) High-resolution TEM micrographs of PdAg nanowires at different magnifications. The scale bars are (A) 20 nm and (B) 5 nm. (C) The high angle annular dark field (HAADF) STEM image of PdAg nanowires and the corresponding elemental mapping of Ag (D), Pd (E). (F) Overlay map of the elements in the PdAg nanowires.

dx.doi.org/10.1021/cs200538g | *ACS Catal.* 2012, 2, 84−90

nanowires, PdAg alloy nanoparticles were first formed and then grow into nanowires.[36,38,39]

The crystalline phase of the PdAg nanowires was further studied with powder XRD measurement. Figure 3 shows the

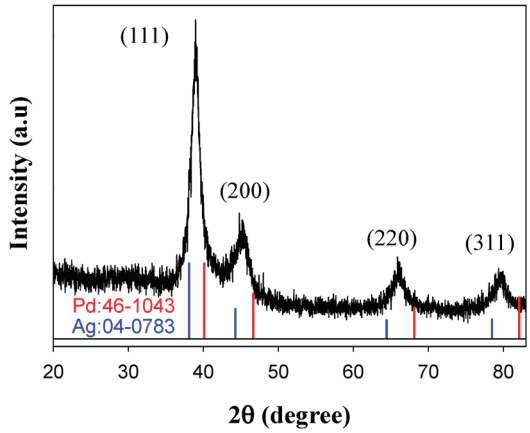

Figure 3. XRD patterns of the as-synthesized PdAg nanowires. For comparison, bulk Pd, Ag from the JCPDS were also included.

XRD pattern of the PdAg nanowires. For comparison, bulk Pd (No. 65-6174) and Ag (No.04-0783) from the Joint Committee on Powder Diffraction Standards (JCPDS) are also included. It can be clearly seen that the nanowires show clear diffraction peaks, corresponding to the (111), (200), (220), and (311) planes as labeled in Figure 3. Compared to the JCPDS data of Pd, the diffraction peaks from PdAg nanowires shift to lower 2θ values, suggesting the reduction in lattice constant. Here, all the diffraction peaks from PdAg nanowires locate between the positions expected for the pure palladium and silver, indicating the obvious alloying of Pd and Ag. Such XRD phenomenon has also been observed with other bimetallic alloy nanostructures.[40−42] Moreover, neither a Pd nor a Ag single component peak was detected, confirming the presence of only single-phase PdAg alloys. It also should be noted that, from the JCPDS file of bulk Pd (No. 65-6174), the intensity ratio between the diffraction peaks of (111) and (200) is 1.44. However, from the XRD pattern of the present PdAg nanowires, the ratio increases to 2.68, suggesting the abundant (111) planes of the PdAg nanowires. Such result is consistent with (111) interplanar spacing found in the HRTEM measurements (Figure 2B).

3.2. Formic Acid Electro-Oxidation with PdAg Alloy Nanowires. The electrocatalytic activity of the as-prepared PdAg nanowires was studied with electrochemical cyclic voltammetry. Figure 4A shows the typical cyclic voltammograms (CVs) of the PdAg alloy nanowires (PdAg-NW/GC) and commercial Pd/C catalyst (Pd/GC) electrodes with the same loading in N_2-saturated 0.1 M $HClO_4$ solution at a potential scan rate of 20 mV/s. From the overall CV profile, it can be seen that electrochemical features of palladium can be observed obviously at PdAg-NW/GC electrode. The oxidation current of palladium appears above +0.4 V in the positive-potential scan. In the reverse scan, the reduction current peak of palladium oxides can be seen at +0.37 V. In the low potential region, there are two pairs of well-defined current peaks at -0.18 and -0.04 V, corresponding to the hydrogen adsorption and desorption. Note that, only one pair of current peaks from hydrogen adsorption, desorption, and evolution are usually

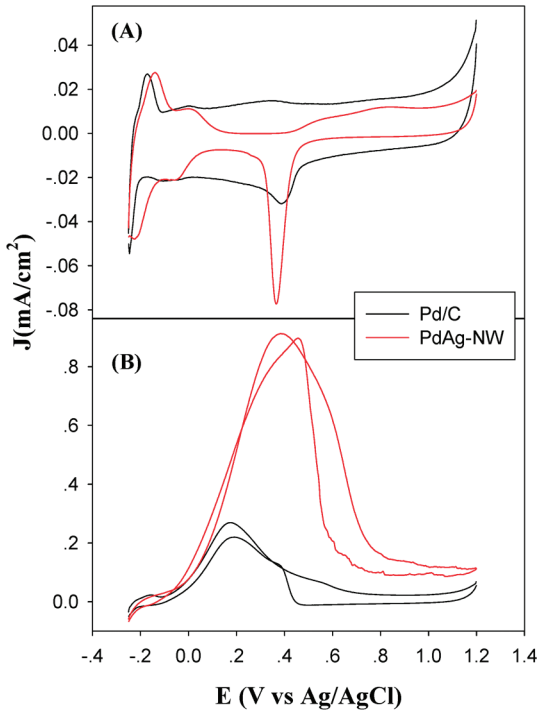

Figure 4. Cyclic voltammograms of the PdAg-NW/GC and Pd/GC electrodes (A) in 0.1 M $HClO_4$ solution and (B) in 0.1 M $HClO_4$ + 0.5 M HCOOH solution. Potential scan rate 20 mV/s.

observed on bulk palladium electrodes. With the present PdAg nanowires, the appearance of two separated hydrogen adsorption and desorption peaks suggests the large surface area of the materials, which has also been observed with other Pd nanostructured materials.[43,44] Such PdAg nanowires with large specific surface area are very favorable in the application of catalysis. Meanwhile, the observed CV features suggest that the as-synthesized PdAg nanowires are electrochemically active. From the CV curve of Pd/C, the voltammetric features are similar to those of PdAg-NW/GC. However, in the potential window between +0.19 and +0.39 V, the double-layer capacitance of Pd/C is much larger than that of PdAg nanowires, which maybe arise from the carbon support material in Pd/C catalyst. Note that compared to the Pd/C catalyst, the hydrogen adsorption/desorption region obtained on PdAg nanowires shifts to more positive potential (i.e., hydrogen is more strongly adsorbed). Such voltammetric response may be ascribed to the charge-transfer in the Pd−Ag alloy structure, leading to the change of hydrogen chemisorption energy.

Figure 4B shows the steady cyclic voltammograms of formic acid oxidation at the PdAg-NW/GC (red curve) and Pd/GC (black curve) electrodes in 0.1 M $HClO_4$ + 0.5 M HCOOH at a potential scan rate of 20 mV/s. It should be noted that the voltammetric currents have been normalized to the actual active surface areas (i.e., electrochemically active surface areas) of the respective electrodes which are calculated by assuming that electrochemical adsorption or desorption of hydrogen yields 210 $\mu C/cm^2$ of Pd surface area. It should be noted that the real active surface area can also be calculated from the palladium oxides reduction charge (424 $\mu C/cm^2$). With such method, the calculated current densities are very close to those shown in Figure 4.

For HCOOH electro-oxidation on both PdAg-NW/GC and Pd/C commercial catalyst, the current density of the anode

dx.doi.org/10.1021/cs200538g | ACS Catal. 2012, 2, 84−90

peak (J_a) is larger than that of the cathodic peak (J_c), qualitatively indicating the much better CO tolerance of Pd nanomaterials than that of Pt-based catalysts[6,45] or no CO poisoning with the Pd catalysts. However, in comparison with the CV profile of Pd/GC electrode, at least two aspects warrant special attention from the CV curve of formic acid oxidation at the PdAg nanowire electrode. First, the current density of formic acid oxidation in both forward and reverse potential sweeps is much larger (about 3.4 times) than that obtained at commercial Pd/C catalysts. Second, the onset potential of formic acid oxidation on PdAg nanowires is a little more negative than that on the Pd/GC electrode. Since the current density and onset potential of fuels oxidation are the two important parameters in the quantitative assessments of electrocatalytic performance, the larger oxidation current density and lower onset potential obtained on PdAg nanowires indicate the as-synthesized alloy nanowires have much better catalytic activity than that of commercial Pd/C catalysts.

The activity and long-term stability of the PdAg nanowires and Pd/C catalysts for formic acid oxidation were further evaluated with chronoamperometric measurements in 0.1 M $HClO_4$ containing 0.5 M HCOOH. Figure 5A–B show the

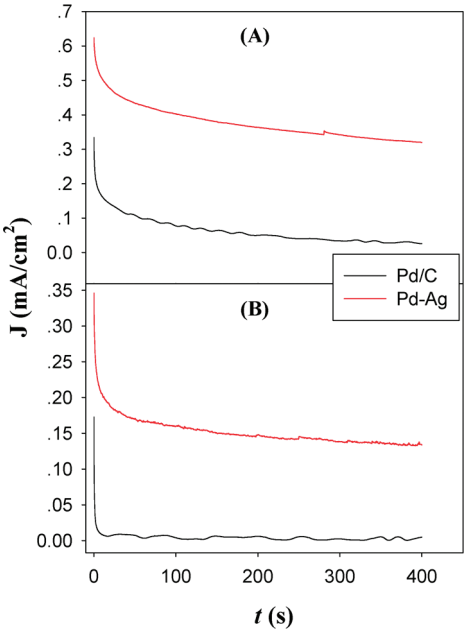

Figure 5. Chronoamperometric curves of the Pd/GC (black curves) and PdAg-NW/GC (red curves) electrodes in 0.1 M $HClO_4$ + 0.5 M HCOOH solution at different electrode potentials: (A) + 0.3 V and (B) + 0.68 V.

chronoamperometric curves at the potentials of +0.3 and +0.68 V, respectively, at PdAg-NW/GC (red lines) and Pd/GC (black lines) electrodes. It can be seen that at both potentials, the maximum initial and steady-state current density obtained with PdAg nanowires is much larger than that on Pd/C catalysts, which agrees well with the result observed from cyclic voltammetric measurements shown in Figure 4B. By analyzing the chronoamperometric curves, it was found that at +0.3 V the current density on PdAg-NW/GC and Pd/GC electrodes decreased to 0.32 and 0.025 mA/cm^2, respectively, at t = 400 s. On the other hand, at +0.68 V, the current density on PdAg-NW/GC and Pd/GC electrodes decreased to 0.13 and 0.0024 mA/cm^2, respectively, at t = 400 s. Compared to the initial maximum current density, the relative value of the decrease for PdAg nanowires is much lower than that for Pd/C. These results indicate that the current density of formic acid oxidation undergoes less decay at the applied constant potentials on the PdAg-NW/GC in the duration time of 400 s. On the basis of the above CV and chronoamperometric evaluations, it can be concluded that the present PdAg nanowires exhibit excellent electrocatalytic performance for formic acid oxidation. Such high catalytic activity may be attributed to the unique nanowire structures with homogeneous alloy domains, where oxygen-containing species adsorbed on Ag sites will enhance the oxidation of formic acid adsorbed on nearby Pd sites. On the other hand, the catalytic activities of metal nanomaterials are dependent strongly on the surface structures. In the previous studies, it has been found that the catalytic activity for formic acid oxidation increases in the order Pd (110) < Pd (111) < Pd (100) in acid electrolytes.[19] Since the above HRTEM and XRD measurements indicated that there exist abundant (111) planes in the present PdAg nanowires, the enhanced catalytic performance may be also attributed to such specific surface properties. Moreover, the synergistic effect between Pd and Ag in the synthesized PdAg nanowires maybe also contributes to their enhanced electrocatalytic activity. The XRD pattern of the PdAg nanowires presented in Figure 3 show that the peaks from Pd shift to lower 2θ values but those of Ag to higher values. Such structurally synergistic effect of PdAg alloys will lead to an electronic structure and a local reactivity much different from that of the monometallic Pd particles.

As a powerful and sensitive technique for studying the kinetics of electron-transfer processes, electrochemical impedance spectroscopy (EIS) has been widely used in electrocatalysis. The dynamics of formic acid electro-oxidation catalyzed by the PdAg nanowires was further examined by EIS measurements. Figure 6A–B shows the Nyquist impedance plots of the PdAg-NW/GC and Pd/GC electrodes, respectively, in 0.1 M $HClO_4$ + 0.5 M HCOOH at different electrode potentials (shown as figure legends). For the PdAg-NW/GC electrode, the impedance spectra show arcs in the first quadrant, and the diameter of the arcs decreases with increasing potential from −0.10 to +0.20 V, suggesting the faster electron-transfer rate of formic acid oxidation at higher potential. In accordance with the impedance, the oxidation current density increases with increasing potential as shown in the CV measurements (Figure 4B). However, with the potential increasing further, the diameter of impedance arcs increases first and then negative impedance was observed in the second quadrant. Such negative impedance has also been found previously in formic acid oxidation on the nanostructured electrocatalysts, and was ascribed to the formation of chemisorbed hydroxyl species at electrode surface.[45−47] At potentials more positive than +0.80 V, the impedance curves return to the normal behavior in the first quadrant. In contrast, all the impedance spectra of Pd/GC electrode are located in the first quadrant within the entire potential range from −0.10 to +0.90 V, as shown in Figure 6B. Such impedance characteristics suggests that there exist only resistive behavior for HCOOH oxidation at the Pd/GC electrode. The lack of (pseudo)-inductive characters of the impedance spectra seems to imply a relatively strong adsorption of CO on Pd/C catalysts and resulting in the slow HCOOH oxidation kinetics.

On the basis of the voltammetric and impedance results, the equivalent circuits shown as inset (a) and (b) in Figure 7 were used to fit the positive and negative impedance spectra,

dx.doi.org/10.1021/cs200538g | ACS Catal. 2012, 2, 84–90

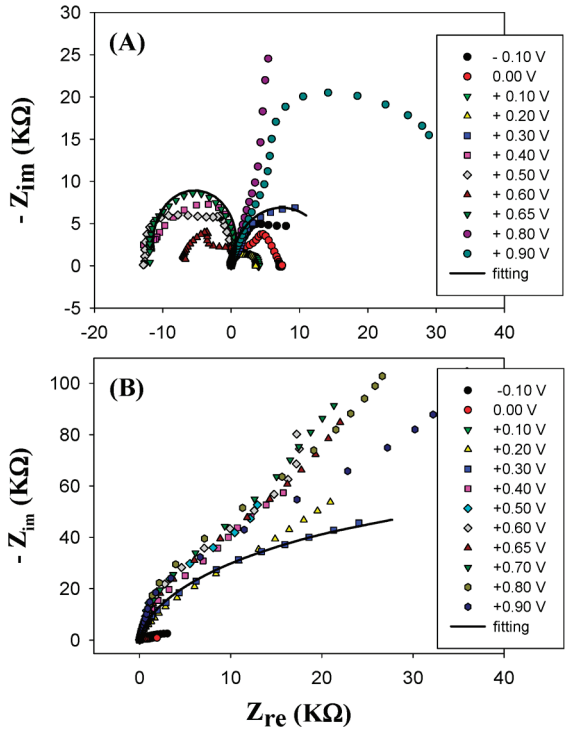

Figure 6. Nyquist impedance plots of formic acid oxidation on PdAg-NW/GC (A) and Pd/GC (B) electrodes in 0.1 M $HClO_4$ + 0.5 M HCOOH at various electrode potentials, which are given in the figure legends. The solid lines show some representative fits to the experimental data based on the equivalent circuits in Figure 7 insets.

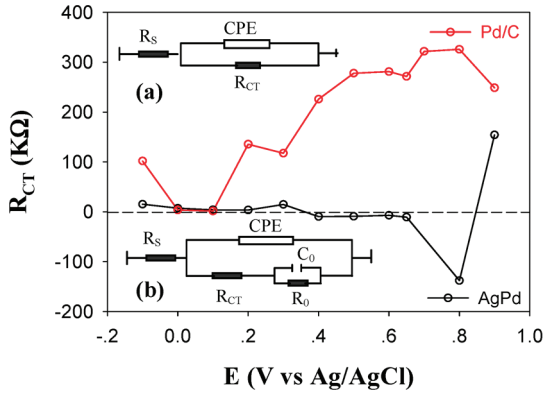

Figure 7. Charge-transfer resistance (R_{CT}) of formic acid electro-oxidation at different electrode potentials on PdAg-NW/GC (black curve) and Pd/GC (red curve) electrodes. Data are obtained from fitting of the electrochemical impedance spectra in Figure 6 with the equivalent circuits (insets). Inset (a) represents the equivalent circuit for normal impedance. Inset (b) is the equivalent circuit for negative impedance.

respectively. Here, R_S represents the solution resistance, CPE (constant-phase element) is the double layer capacitance, R_{CT} is the charge transfer resistance, C_0 and R_0 represent the capacitance and resistance of the electro-oxidation of adsorbed CO intermediates, respectively. The representative fits (solid black lines) for the electrodes were shown in the Nyquist plots in Figure 6, all of which agree well with the experimental data. From the fitting, the variation of the charge transfer resistance (R_{CT}) with the potentials on the electrodes was shown in Figure 7. It can be seen that within the studied potential window, the R_{CT} derived from PdAg-NW/GC is remarkably smaller than that from the Pd/GC electrode. Since charge transfer resistance is one of the main parameters to evaluate the inherent speed of the charge transfer step of an electrode reaction, the smaller R_{CT} indicates that the electron-transfer kinetics for formic acid oxidation at the PdAg nanowires is much better facilitated than that at the Pd/C catalysts.

4. CONCLUSIONS

In this paper, we demonstrate a facile one-step method for preparing alloy PdAg nanowires. From the TEM, HRTEM, and EDX measurements, the as-synthesized nanowires exhibit homogeneous Pd−Ag alloy nanostructures with multiple crystalline domains. The XRD pattern showed that the PdAg nanowires are predominated with Pd (111) planes. The unique nanostructure with large surface area and active surface crystalline facets makes them promising electrocatalysts for direct-liquid fuel cells. In cyclic voltammetric studies of formic acid oxidation, in comparison with the commercial Pd/C catalysts, the as-synthesized PdAg nanowires exhibit much higher catalytic activity with larger oxidation current density, higher CO tolerance, and more negative onset potential. The chronoamperometric analyses indicate that PdAg nanowires have higher long-term stability than Pd/C catalysts. The electron transfer kinetics of HCOOH oxidation on the PdAg nanowires was studied with electrochemical impedance spectroscopy (EIS). The result showed that charge transfer resistance (R_{CT}) obtained on PdAg nanowires is much smaller than that from commercial Pd catalysts, suggesting the highly facilitated electron-transfer kinetics for formic acid oxidation at the synthesized PdAg nanowires. Overall, the present study not only provides a facile method to synthesize alloy metal nanowires, but also finds a kind of novel anode electrocatalyst with high catalytic performance for application in fuel cells.

AUTHOR INFORMATION

Corresponding Author

*E-mail: weichen@ciac.jl.cn.

Funding

This work was supported by the National Natural Science Foundation of China (No. 21043013) and the startup funds for scientific research, Changchun Institute of Applied Chemistry, Chinese Academy of Sciences.

REFERENCES

(1) Wasmus, S.; Kuver, A. *J. Electroanal. Chem.* **1999**, *461* (1−2), 14−31.
(2) Lemons, R. A. *J. Power Sources* **1990**, *29* (1−2), 251−264.
(3) Steele, B. C. H.; Heinzel, A. *Nature* **2001**, *414* (6861), 345−352.
(4) Chen, W.; Chen, S. W. *Angew. Chem., Int. Ed.* **2009**, *48* (24), 4386−4389.
(5) Chen, A. C.; Holt-Hindle, P. *Chem. Rev.* **2010**, *110* (6), 3767−3804.
(6) Chen, W.; Kim, J.; Sun, S. H.; Chen, S. W. *Phys. Chem. Chem. Phys.* **2006**, *8* (23), 2779−2786.
(7) Chen, W.; Kim, J. M.; Xu, L. P.; Sun, S. H.; Chen, S. W. *J. Phys. Chem. C* **2007**, *111* (36), 13452−13459.
(8) Chu, D.; Gilman, S. *J. Electrochem. Soc.* **1996**, *143* (5), 1685−1690.
(9) Chen, W.; Kim, J. M.; Sun, S. H.; Chen, S. W. *J. Phys. Chem. C* **2008**, *112* (10), 3891−3898.
(10) Chen, W.; Xu, L. P.; Chen, S. W. *J. Electroanal. Chem.* **2009**, *631* (1−2), 36−42.

(11) Chen, W.; Chen, S. W. *J. Mater. Chem.* **2011**, *21* (25), 9169–9178.
(12) Bianchini, C.; Shen, P. K. *Chem. Rev.* **2009**, *109* (9), 4183–4206.
(13) Arenz, M.; Stamenkovic, V.; Ross, P. N.; Markovic, N. M. *Surf. Sci.* **2004**, *573* (1), 57–66.
(14) Okada, T.; Miyake, H.; Samjeske, G.; Osawa, M. *Phys. Chem. Chem. Phys.* **2008**, *10* (25), 3662–3669.
(15) Wang, L. Q.; Meng, H.; Shen, P. K.; Bianchini, C.; Vizza, F.; Wei, Z. D. *Phys. Chem. Chem. Phys.* **2011**, *13* (7), 2667–2673.
(16) Zhu, Y.; Kang, Y. Y.; Zou, Z. Q.; Zhou, Q.; Zheng, J. W.; Xia, B. J.; Yang, H. *Electrochem. Commun.* **2008**, *10* (5), 802–805.
(17) Rice, C.; Ha, R. I.; Masel, R. I.; Waszczuk, P.; Wieckowski, A.; Barnard, T. *J. Power Sources* **2002**, *111* (1), 83–89.
(18) Larsen, R.; Ha, S.; Zakzeski, J.; Masel, R. I. *J. Power Sources* **2006**, *157* (1), 78–84.
(19) Hoshi, N.; Kida, K.; Nakamura, M.; Nakada, M.; Osada, K. *J. Phys. Chem. B* **2006**, *110* (25), 12480–12484.
(20) Baldauf, M.; Kolb, D. M. *J. Phys. Chem.* **1996**, *100* (27), 11375–11381.
(21) Xu, C. W.; Wang, H.; Shen, P. K.; Jiang, S. P. *Adv. Mater.* **2007**, *19* (23), 4256–4259.
(22) Yin, Z.; Zheng, H. J.; Ma, D.; Bao, X. H. *J. Phys. Chem. C* **2009**, *113* (3), 1001–1005.
(23) Jia, F. L.; Wong, K. W.; Zhang, L. Z. *J. Phys. Chem. C* **2009**, *113* (17), 7200–7206.
(24) Wang, X. G.; Wang, W. M.; Qi, Z.; Zhao, C. C.; Ji, H.; Zhang, Z. H. *J. Power Sources* **2010**, *195* (19), 6740–6747.
(25) Lim, B.; Jiang, M. J.; Camargo, P. H. C.; Cho, E. C.; Tao, J.; Lu, X. M.; Zhu, Y. M.; Xia, Y. N. *Science* **2009**, *324* (5932), 1302–1305.
(26) Yuan, Q.; Zhou, Z. Y.; Zhuang, J.; Wang, X. *Chem. Mater.* **2010**, *22* (7), 2395–2402.
(27) Yuan, Q.; Zhuang, J.; Wang, X. *Chem. Commun.* **2009**, *43*, 6613–6615.
(28) Guo, S. J.; Dong, S. J.; Wang, E. K. *Energy Environ. Sci.* **2010**, *3* (9), 1307–1310.
(29) Teng, X. W.; Feygenson, M.; Wang, Q.; He, J. Q.; Du, W. X.; Frenkel, A. I.; Han, W. Q.; Aronson, M. *Nano Lett.* **2009**, *9* (9), 3177–3184.
(30) Habas, S. E.; Lee, H.; Radmilovic, V.; Somorjai, G. A.; Yang, P. *Nat. Mater.* **2007**, *6* (9), 692–697.
(31) Sun, Y. G. *Nanoscale* **2010**, *2* (9), 1626–1642.
(32) Sun, Y. G.; Tao, Z. L.; Chen, J.; Herricks, T.; Xia, Y. N. *J. Am. Chem. Soc.* **2004**, *126* (19), 5940–5941.
(33) Lu, Y. Z.; Jin, R. T.; Chen, W. *Nanoscale* **2011**, *3* (6), 2476–2480.
(34) Lu, Y. Z.; Chen, W. *J. Phys. Chem. C* **2010**, *114* (49), 21190–21200.
(35) Liu, Q. S.; Yan, Z.; Henderson, N. L.; Bauer, J. C.; Goodman, D. W.; Batteas, J. D.; Schaak, R. E. *J. Am. Chem. Soc.* **2009**, *131* (16), 5720–5721.
(36) Peng, Z. M.; You, H. J.; Yang, H. *ACS Nano* **2010**, *4* (3), 1501–1510.
(37) Wang, C.; Hou, Y. L.; Kim, J. M.; Sun, S. H. *Angew. Chem., Int. Ed.* **2007**, *46* (33), 6333–6335.
(38) Tang, Z. Y.; Kotov, N. A. *Adv. Mater.* **2005**, *17* (8), 951–962.
(39) Cademartiri, L.; Ozin, G. A. *Adv. Mater.* **2009**, *21* (9), 1013–1020.
(40) Wanjala, B. N.; Luo, J.; Loukrakpam, R.; Fang, B.; Mott, D.; Njoki, P. N.; Engelhard, M.; Naslund, H. R.; Wu, J. K.; Wang, L. C.; Malis, O.; Zhong, C. J. *Chem. Mater.* **2010**, *22* (14), 4282–4294.
(41) Huang, J. C.; Liu, Z. L.; He, C. B.; Gan, L. M. *J. Phys. Chem. B* **2005**, *109* (35), 16644–16649.
(42) Lu, Y. Z.; Chen, W. *Chem. Commun.* **2011**, *47* (9), 2541–2543.
(43) Pan, W.; Zhang, X. K.; Ma, H. Y.; Zhang, J. T. *J. Phys. Chem. C* **2008**, *112* (7), 2456–2461.
(44) Zhang, J. T.; Huang, M. H.; Ma, H. Y.; Tian, F.; Pan, W.; Chen, S. H. *Electrochem. Commun.* **2007**, *9* (6), 1298–1304.
(45) Chen, W.; Kim, J. M.; Sun, S. H.; Chen, S. W. *Langmuir* **2007**, *23* (22), 11303–11310.
(46) Hsing, I. M.; Wang, X.; Leng, Y. J. *J. Electrochem. Soc.* **2002**, *149* (5), A615–a621.
(47) Chen, A. C.; La Russa, D. J.; Miller, B. *Langmuir* **2004**, *20* (22), 9695–9702.